The Use of Pressure Fluctuations on the Nose of an Aircraft for Measuring Air Motion

E. N. BROWN, C. A. FRIEHE[1] AND D. H. LENSCHOW

Research Aviation Facility, National Center for Atmospheric Research,[2] Boulder, CO 80307

(Manuscript received 12 April 1982, in final form 18 August 1982)

ABSTRACT

An air-motion sensing technique is described for measurement of attack and sideslip angles and dynamic pressure. The sensing probe consists of an array of five pressure holes in the standard radome of a twin-jet research aircraft. Comparisons are made with air motion measurements (angle of attack and dynamic pressure) obtained from a conventional differential pressure flow angle sensor at the tip of a nose boom 1.5 fuselage diameters ahead of the aircraft body. The results indicate that the radome system works well down to scale sizes slightly larger than the fuselage diameter. (Finer scale measurements were limited by pressure transducer response.) An *in-situ* calibration technique is described for the determination of the empirical radome angle–pressure difference sensitivity factor k, as a function of aircraft Mach number. The value of k, so determined at low Mach numbers, is in approximate agreement with that calculated for potential flow for a spherical radome. The *in-situ* technique applied to the conventional nose boom sensor indicates that the value of k based on wind tunnel calibrations may not apply for the present installation.

The time response of the conventional pressure system on the NCAR Sabreliner twin-jet aircraft is estimated on the basis of an in-flight comparison between the conventional pressure probe and a fast-response gust probe flown together on a nose boom. Comparison of the power spectra of the conventional and radome angles of attack for a traverse in boundary-layer turbulence indicates that the response of the radome system is superior to the conventional system due to the shorter pressure lines that can be used.

1. Introduction

The use of research aircraft to measure atmospheric motions, from mean horizontal winds to turbulent eddies, has improved greatly in the last few decades. Measurement techniques have evolved along two lines: 1) use of the aircraft's response to winds, and 2) the installation of a variety of velocity sensors on the tips of long nose booms ahead of the aircraft. Aircraft response techniques are presented by Lenschow (1976) and Lawson (1979), for example, and we will not discuss them further. Booms are generally mounted in front of the fuselage of the aircraft (on or close to the roll axis to minimize roll-induced velocity), and the lengths are typically 1.5 times the fuselage diameter. The origin of this rule-of-thumb formula for the length is not easily traceable, but apparently has evolved from limited tests on a military aircraft (McFadden *et al.*, 1952). It can be shown (Lenschow *et al.*, 1978) that, assuming potential flow, the reduction in airspeed, 1.5 diameters ahead of a body obtained by rotating the curve (in polar coordinates)

$$r = a/(\sin \tfrac{1}{2}\theta)$$

about an axis parallel to a flow field that is uniform $(u = -U)$ for $r = (x^2 + y^2)^{1/2} \to \infty$, is ~2%, with the error decreasing as the square of the inverse distance from the front of the body. Similarly, the error in flow angle 1.5 diameters out from the body at an angle of $\theta = 30°$ from the polar axis, is ~0.6°. [For a recent discussion of a technique for evaluating distortion effects on turbulence measurements, see Wyngaard (1981).] Various sensors are placed at the boom tip to measure velocity components, e.g., pitot tubes/vanes, multihole pressure probes, hot-wire anemometers, or sonic anemometers. Sensor performance is degraded if boom vibrations are significant. In some designs, an inner nose boom, isolated from the outer boom by shock and vibration isolators, rigidly couples the air motion sensors to an inertial navigation unit (INU) in the nose of the aircraft for precise measurement of boom motion as well as isolation of the air sensors and the INU from aircraft vibrations.

In this paper, we present an alternative technique for the measurement of air motion: the measurement of the surface pressure distribution on the nose of the aircraft itself, from which, by suitable calibrations, the angles of attack and sideslip, and the dynamic pressure can be obtained. Here we define the angles of attack and sideslip as the flow angles of the air with respect to the longitudinal axis of the airplane in the vertical and lateral directions (with respect to the airplane axes), respectively. Attack angle is positive

[1] Present affiliation: Department of Mechanical Engineering, University of California, Irvine 92717.

[2] The National Center for Atmospheric Research is sponsored by the National Science Foundation.

when the flow impinges on the aircraft from below, and sideslip is positive for a clockwise rotation (when viewed from above). These angles and the true airspeed, which is calculated from the dynamic pressure, air temperature and static pressure, define the velocity vector relative to the aircraft. Combining this with data on the aircraft motion with respect to the earth (as measured by an INU, for example), we can calculate the wind vector with respect to the earth (see Lenschow, 1972, for the general principles).

We wished to develop an extremely simple air-motion system that would not interfere with storm-avoidance or research radar in the nose of the aircraft. On several NCAR aircraft, the INU-coupled inner boom systems severely limit or preclude radar use. Thin pipe booms mounted off the nose can be used in conjunction with radar, but considerable structural modifications are required, and vibration can be a serious problem. It may, in fact, limit high-frequency air-motion measurements to an extent that precludes measurement of turbulent fluxes.

The National Aeronautics and Space Administration (NASA) pioneered the proposed technique in the 1960's. Angles of attack and sideslip were measured on the Mach 7 X-15 vehicle from an array of pressure holes placed in a 30-cm titanium sphere mounted in the nose (Fischel and Webb, 1964). The differential pressure signals (from ports at $\mp 42°$ from the centerline of the sphere, one set for attack and one for sideslip) were fed to a servosystem, and the sphere was rotated (in two directions) until nulls were measured. The attack and sideslip angles were read out from position indicators. Dynamic pressure was measured separately from a fuselage-mounted Pitot and fuselage static pressure source. This unique system did not require that the pressure distribution around the spherical element be known, as the angles were measured when the differential attack and sideslip pressures on the sensor were zero. The measured angles, however, may still be subject to error introduced by the aircraft upwash, so that the measured angles may not be the actual attack and sideslip angles with respect to the unmodified flow field far removed from the aircraft.

NASA has also investigated the use of an array of fixed holes on the nose of an aircraft, as recently proposed for use on the Space Shuttle (FADS, Flush Air Data System). Larson and Siemers (1978) performed model wind tunnel tests and flight tests on a KC-135 and determined that the pressure distribution was a monotonic function of attack and sideslip. It was concluded that the FADS was feasible for mean attack and sideslip angle measurements.

The use of the pressure distribution around a fixed body of revolution to measure incident flow angles has been known for some time. Probes for this purpose were apparently first developed by van der Hegge-Zijen (see Eckert, 1938). At least one commercial version for aircraft is available currently. In high Reynolds number flow past a sphere ($\mathrm{Re} \equiv Ud/\nu$, U = free stream velocity, d = sphere probe diameter, ν = kinematic viscosity), the pressure distribution for potential flow is (see Fig. 1)

$$P_\theta - P_\infty = \frac{1}{2}\rho U^2\left(1 - \frac{9}{4}\sin^2\theta\right), \qquad (1)$$

where P_θ = pressure at angle θ, P_∞ = static pressure, and ρ = fluid density. Since the probes are usually used in high Reynolds number flows, the pressure drop across the extremely thin viscous boundary layer on the surface of the probe nose is negligible, and (1) is expected to hold, based on inviscid flow theory. Montoya (1973), and Armistead and Webb (1973) presented wind tunnel and flight tests for hemispherical probes over a range of Mach numbers, M. In general, the wind tunnel results support (1) up to $M \approx 0.5$. For $M > 0.5$, compressibility effects alter (1), but the probe can still be used to measure flow angles because the pressure distribution is a monotonic function of θ, although not predictable by potential flow theory. The sensitivity of P_θ to change in angle is obtained by differentiating (1) with respect to θ, and we see that maximum sensitivity is obtained for $\theta = \mp 45°$. Most commercial probes, therefore, have two sets of holes (one for attack and one for sideslip) at $\mp 45°$ on the hemispherical tip of the cylinder. A center hole and static holes around the cylindrical portion are added for measurement of total and static pressures.

We measured pressures and pressure differences from five holes placed in the radome of a twin-jet research aircraft and compared the data measurements from a commercial pressure sensor on the boom of the aircraft. At the outset, it may seem that flow distortion effects at the nose of the aircraft would invalidate the technique. There, the velocity field is strongly distorted which alters the pressure field. We use this distortion of the pressure field by the aircraft body to infer the undistorted velocity field away from the body. The velocity at the surface of the aircraft

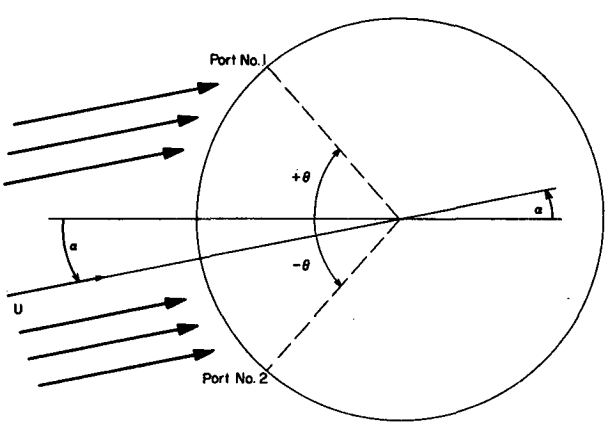

FIG. 1. Sketch of flow around a sphere indicating attack angle α and angles of pressure taps on sphere surface θ.

nose is zero, but the pressure at the surface is, within the Prandtl boundary-layer approximation, equal to that outside the boundary-layer in the inviscid flow. Because of the extremely high Reynolds number of the aircraft motion through the atmosphere, the boundary-layer approximation should be excellent if the pressure holes are positioned at short distances from the stagnation point on the nose. Therefore, the surface pressure pattern will be related to the free-stream velocity through an equation similar to (1).

The above arguments are expected to hold for laminar flow in the airstream, or mean motion in a turbulent airstream. But, it is of interest to measure the turbulent motions as well in atmospheric research. Two questions now arise: how are turbulent eddies distorted as the aircraft approaches, and is the fluctuating pressure signal on the surface related to the undistorted fluctuating motion in the freestream? The works of Hunt (1973), Britter *et al.* (1979), Durbin and Hunt (1980), and J. Wyngaard (private communication, 1982) are useful in this regard. Hunt (1973) has shown there are two limiting types of flow distortion of turbulence past bluff bodies. For the case of turbulent scales larger than the body, the body "blocks" the flow, and the distortions are irrotational. For scales smaller than the body, the eddies are distorted by a straining field as they approach the body. For the aircraft case, where the fuselage diameter is ~2–3 m, we are interested in eddies of this scale and larger, so the "blockage" mechanism dominates. Eddies of this scale and larger resolve the turbulent fluxes and the inertial-subrange region of the spectra in most situations.

Durbin and Hunt, and Wyngaard have shown that, for the "blockage" case, the surface pressure fluctuations are related through a Bernoulli-type equation to the free-stream velocity fluctuations. This means that in principle the pressure holes on the surface of the aircraft can act as an "anemometer" for mean and turbulent motions, at least down to some scale size comparable to the aircraft body size. The theoretical "blockage" results are for the limiting case of eddy sizes much larger than the body size. The practical limit of the smallest eddies that can be measured without significant distortion remains to be determined by comparative experiment.

2. Theory of measurement

From (1), the normalized pressure $\hat{P} \equiv P/(\frac{1}{2}\rho U^2)$, where $q = \frac{1}{2}\rho U^2$, at each of the two attack ports on a sphere (Fig. 1) for an attack angle α is

$$\hat{P}_1 - \hat{P}_\infty = 1 - \frac{9}{4}\sin^2(\theta + \alpha), \tag{2}$$

$$\hat{P}_2 - \hat{P}_\infty = 1 - \frac{9}{4}\sin^2(\theta - \alpha). \tag{3}$$

The pressure difference between the two ports is

$$\Delta\hat{P} \equiv \hat{P}_1 - \hat{P}_2 = \frac{9}{4}[\sin^2(\theta - \alpha) - \sin^2(\theta + \alpha)] \tag{4}$$

$$= -\frac{9}{4}\sin 2\theta \sin 2\alpha. \tag{5}$$

From (5), we see that maximum sensitivity occurs at $\theta = \pm \pi/4$. For small attack angles, (5) can be solved for α and expanded in the series (using $\theta = -\pi/4$)

$$\alpha = \frac{2}{9}\Delta\hat{P} + \frac{16}{2187}(\Delta\hat{P})^3 + \frac{64}{98415}(\Delta\hat{P})^5 + \cdots. \tag{6}$$

A sensitivity factor k is commonly defined as

$$\alpha = k^{-1}\Delta\hat{P}, \tag{7}$$

for α measured in degrees. Using only the first term in the expansion (6),

$$k = 0.078.$$

The error in using only the first term in this expansion is <5% for $|\alpha| < 15°$.

As mentioned above, the value of $k = 0.078$ appears to have been reasonably verified in wind tunnel tests (Vornwald, 1981) for $M < 0.5$. There is some evidence (see, e.g., Rogal, 1964) that for $M < 0.3$, the value of k is less than the theoretical value.

In the present application, the shape of the front of the test aircraft is spherical for a small region at the nose tip. We have not calculated the potential flow about the complex aircraft shape, so we cannot derive a theoretical value for k. However, we will test and analyze our results using (7), with the values of k and M dependence to be determined by experiment.

3. Test configuration

The test aircraft was the NCAR Model 65 Sabreliner, fitted with a Rosemount Eng. Co. 858AJ28 five port pressure sensor at the tip of the 3.04-m nose boom for flow-angle and dynamic pressure measurements. The fuselage diameter is 2.01 m, which places the boom tip at 1.51 diameters ahead of the nose (see Fig. 2). Pressure transducers for the boom sensor are located in the nose section behind the radome, connected by 4.0 m of tubing.

The radome (in the vertical plane, Fig. 3) was de-

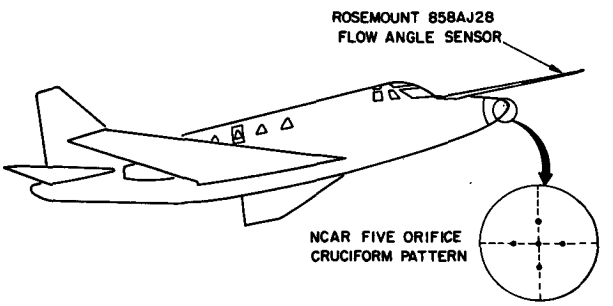

FIG. 2. Sketch of test aircraft showing conventional nose boom and detail of pressure taps in radome.

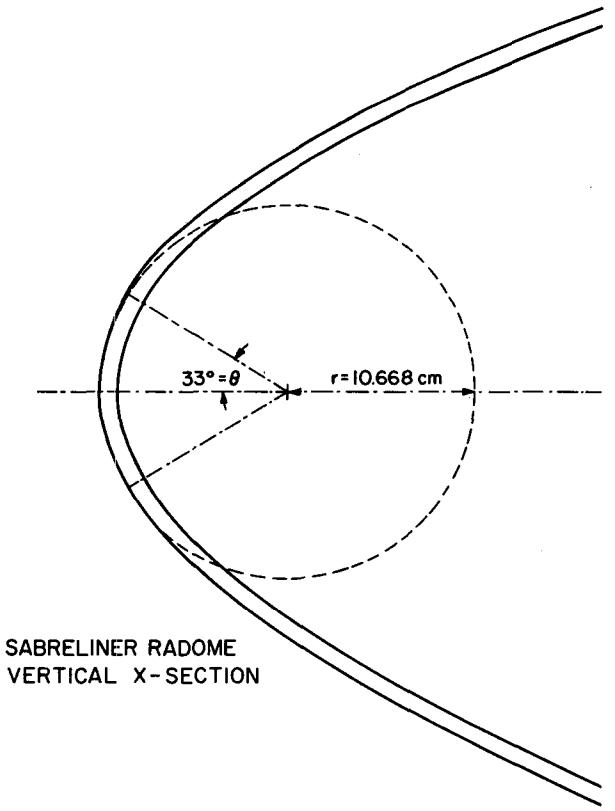

FIG. 3. Vertical cross section of radome showing circular portion and position of attack pressure holes.

termined to be spherical to ∓33°. Five 0.64-cm-diameter holes were drilled in the tip of the radome, each normal to the local tangent at 0° and ∓33° for total dynamic pressure and attack and sideslip pressure differences, respectively. The holes were referenced with a transit to the aircraft using the wings and vertical stabilizer as references. The radome is slightly flattened and is not symmetric about the horizontal plane; its overall shape and the location of the five pressure ports is shown in Fig. 4 along with the boom.

Type 11 nylon tubing was put through the radome holes from the inside and cemented into place; the tube ends were contoured to the radome surface to achieve burr-free ports 0.43 cm in diameter. The tubes between the pressure transducers and the radome were 1 m long, considerably less than for the 858 probe. Comparisons of the 858 probe and radome configurations are given in Table 1. As is shown in Table 1, the sizes of the ports may be significant; the theory, of course, assumes infinitesimal pressure ports.

The static pressure from the 858 probe is obtained from a ring of pressure holes approximately 2.5 diameters behind the probe tip. For the radome system, the manifolded aircraft fuselage static source (approximately 2.2 m behind the radome tip) was used. Rosemount Eng. Co. 1201 (absolute) and 1221 (differential) pressure transducers were used. Pressure data, temperatures, inertial navigation data, etc., were recorded on a digital computer-compatible tape *via* a specially developed aircraft data acquisition system (Duncan and Brown, 1978). The pressure data were filtered with a four-pole Butterworth low-pass filter (−3 dB at 10 Hz) to reduce aliasing and sampled at 25 s^{-1}.

Pressure transducers were calibrated before and after the test flights against a traceable standard accurate to ∓0.2 mb (∓20 Pa). Data system resolution of the attack and sideslip pressure differences was 2.5 Pa. Static pressure corrections for the boom and fuselage, and temperature recovery factors were obtained by flying past the NOAA Boulder Atmospheric Observatory 300-m tower.

4. Flight test plan

A variety of maneuvers was flown in nonturbulent conditions to evaluate the radome differential pressure method and make comparisons with the 858 probe. Constant Mach number runs of three minutes duration at constant altitude were made after stable aircraft conditions were observed. The airplane performed pushovers and pullups (attack maneuvers) at M = 0.3, 0.4 and 0.5 at pitching rates of 0.5° s^{-1}. Except for these maneuvers, the airplane was flown in a clean configuration and near 1-g conditions. A slow deceleration run was flown in quiescent meteorological conditions to provide a continuous variation of Mach number from 0.67 to 0.21, which gave attack angle variations of 2 to 15°.

A data set in light to moderate turbulence was obtained from a boundary layer flight below 300 m altitude.

Some forced, uncoordinated maneuvers for sideslip were performed, but were limited by operating restrictions on the Sabreliner. Therefore, we present mainly angle of attack data in this paper.

5. Results

a. Maneuver results

A comparison of the 858 and radome attack pressure signals versus time recorded during a 15-min maneuver period is shown in Fig. 5. The variations in the traces are similar, down to the smallest details (except for the very last portion of the 15-min time period, which will be explained later). The radome pressure difference signal (ADIFR) responded at least as well as the corresponding 858 boom signal (ADIF), during both the forced maneuvers and the "quiescent" periods in between. However, the magnitude of the peaks during the maneuvers are different. The radome peak-to-peak amplitude is ~83% that of the 858. Part of this is due to the differences in the angles between the ports. If we consider both the radome and the 858 to be spherical probes with holes at θ

FIG. 4. Photograph of NCAR Sabreliner Model 65 showing nose boom with 858 pressure sensor and pressure holes in radome.

= 33 and 45°, respectively, (5) predicts that the radome peak-to-peak amplitude in the above maneuver case would be 91% of the 858. The approximate agreement with potential flow theory is encouraging. Similar results, but with different magnitude ratios, were found for the limited sideslip maneuvers.

The radome system can be calibrated *via* (5) by using the 858 probe data to independently measure the angle α. This would involve using the recommended factory calibration for the 858 probe. However, to fully demonstrate the utility of the radome system, we have developed an *in-situ*, calibration procedure which does not require an independent measurement of attack angle. (The need for an independent angle-of-attack system for calibration would detract from the simplicity of the proposed radome system, as it would probably involve a boom.) The technique is basically to use selected times of the data set when the plane is flying in relatively smooth air away from meteorological disturbances such as the boundary layer, clouds and jet streams. Under these quiescent conditions, the change in aircraft altitude, etc., is carefully monitored so that the assumption of zero vertical wind and aircraft vertical velocity can be made. Then we can substitute pitch angle (which is accurately and precisely measured by the inertial navigation system) for attack angle in (7). In this way we are also able to obtain an *in-situ* calibration for the 858 probe for comparison with the recommended formula based on wind tunnel studies for the probe alone.

TABLE 1. 858AJ and radome measurements.

Sensor	Diameter (cm)	Orifice locations	Orifice diameter (cm)	Angle subtended by orifice
858AJ	2.54	∓45°	0.16	7.2°
		0° (Pitot)	0.40	17.5°
Radome	21.3*	∓33° (All)	0.43	2.3°

* Diameter of spherical portion of radome nose.

In order to develop a complete radome-based air motion system, we need to obtain the dynamic pressure which also appears in (7). As can be expected, there is not a good static pressure source on the radome; instead, we have used the aircraft's fuselage static ports, as mentioned previously. The total pressure at the center port of the radome is sensitive to angle; i.e., the center hole is not a good Pitot hole. In most Pitot-static tube designs, the dynamic pressure is insensitive to angles within $\sim \pm 10°$. In fact, insensitivity to attack angle, which is desirable in a Pitot tube, requires quite different design criteria. An

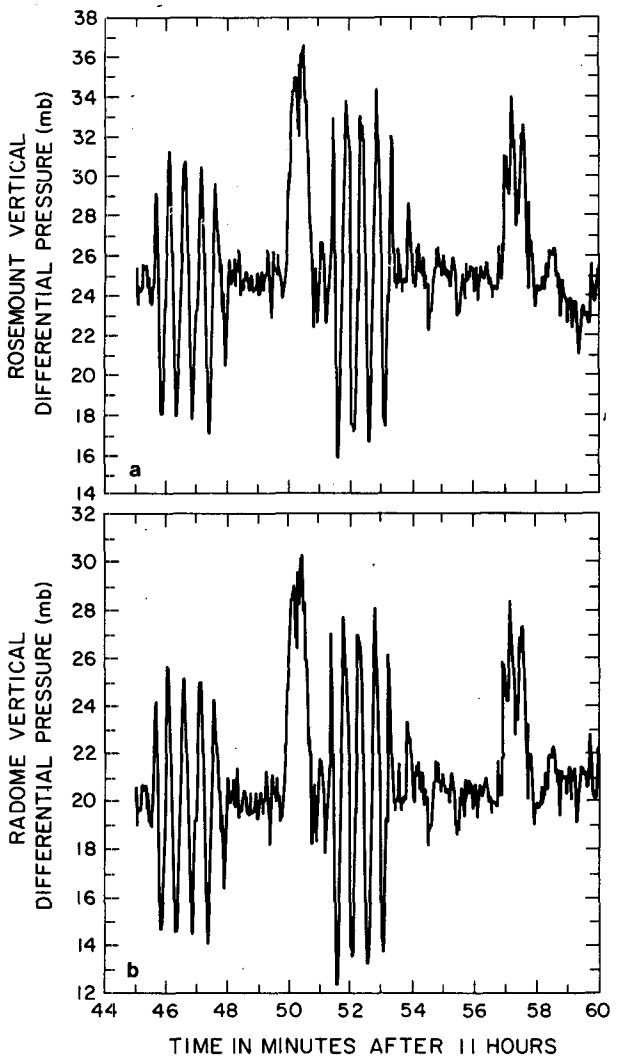

FIG. 5. Time series of attack pressure differences for Rosemount 858 (a) and radome (b).

open-ended cylinder with little or no streamlining at the tip is much less sensitive to attack angle than a hemispherical probe with a small hole at the tip. We have developed a correction scheme for the radome total pressure whereby, for each recorded sample of data, the flow angle is estimated *via* (7) with a k value for a sphere and $\theta = 33°$. Then the total pressure at the center hole is increased [*via* (1)] to approximately correct the measured pressure to zero attack (and sideslip) angle. The corrected radome pressures (QCRC) are compared with the reference aircraft dynamic pressures from the fuselage Pitot (QCFC) in Fig. 6. Here, the top curve shows the attack angle versus time in a deceleration run (i.e., M is continuously decreasing along the curve). The middle curve shows the ratio of the uncorrected radome dynamic pressure QCR to QCFC. Several-percent errors are obtained at moderate angles of attack. The results of the correction procedure described above are shown in the bottom curve and show the percent error is small out to attack angles of $\approx 10°$. Angles greater than 10° are out of the normal Sabreliner operating envelope, so this deviation is not significant.

b. k *values*

From selected data under quiescent conditions at different Mach numbers, k values were obtained from the measured pressure differences, pitch angles and corrected radome dynamic pressures. The variation of k and M is shown in Fig. 7. There is some scatter, and the least-squares fit line shows a linear decrease in k with M. Also shown in Fig. 8 are two sets of k values for the 858 probes: the upper curve is the factory recommendation (which has $k = 0.078$, the theoretical value, at low Mach numbers and a decrease in k for $M > 0.5$). The other data set for the 858 probe is that obtained by the *in-situ* technique described above for the radome applied to the 858 data. (For the 858, the total pressure was not corrected for angle sensitivity, and the static pressure was obtained from the 858 static pressure taps.) The *in-situ* calibration gives a lower k value, with approximately the same shape versus Mach number as the wind tunnel calibration curve. This is perhaps indicative of flow distortion at the location of the 858; 1.53 diameters ahead of the fuselage may not be far enough, or possibly the boom itself distorts the air flow. The lower value of k does correspond to the effect of divergent streamlines around the boom tip: pitching the probe in this flow would give an apparent greater angular

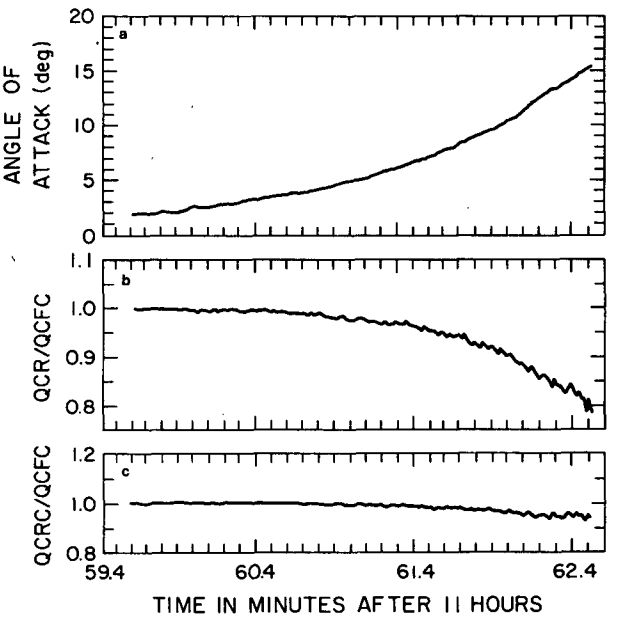

FIG. 6. Time series of attack angle (a), ratio of radome dynamic pressure to corrected fuselage pressure, QCR/QCFC (b), and corrected radome dynamic pressure to corrected fuselage pressure, QCRC/QCFC (c).

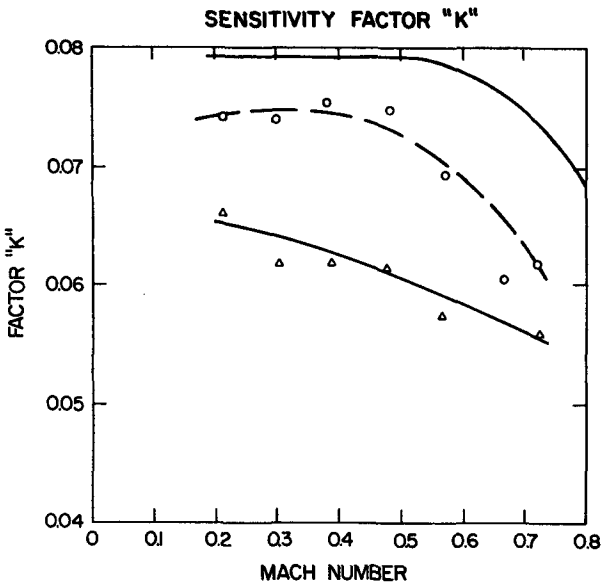

FIG. 7. Sensitivity factor k versus Mach number. Solid line: recommended factory calibration for Rosemount 858 probe. Dashed line with circles: measured in-situ values for 858 probe on the NCAR Sabreliner. Solid lines with triangles: measured in-situ values for radome.

sensitivity (lower k) than in the undisturbed case. Also, the local static pressure at the 858 has been found to be greater than the free-stream undistorted value. Therefore, if the total pressure is unaffected, the value of q in (7) will be less and k would have to be increased to obtain the correct α for the measured $\Delta\hat{P}$. Apparently, in the particular configuration studied, the first effect dominates the static pressure defect.

The lower, *in-situ* values of k for the 858 probe on the Sabreliner agree with previous results of Armistead and Webb (1973), who performed *in-situ* flight tests on a F-104 aircraft.

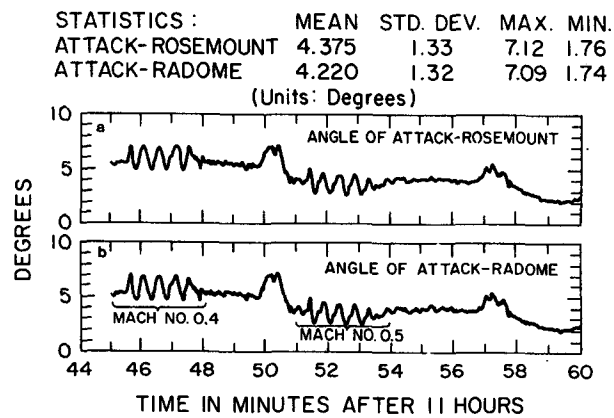

FIG. 8. Comparison of angle of attack computed for data of Fig. 5. (a) Rosemount 858 probe; (b) Radome. The correlation coefficient between the two attack angles is 0.99917 with an offset of 0.2°.

From the limited sideslip data, the *in-situ* k value for the 858 probe was found to be 0.068 for $M = 0.4$ and 0.5; the value for the radome was 0.04, significantly lower. The low value is believed to be caused by the significantly different shape of the radome in the horizontal plane.

Finally, we have determined that there is negligible crosstalk between the radome attack and sideslip pressure difference data. That is, the total vector angle of the wind, relative to the aircraft, can be resolved into the attack plane and the sideslip plane and these can be calculated independently. Our flight data to support this are necessarily limited as we cannot independently vary α and β (sideslip) angles over the full $-10°$ to $+10°$ range for all Mach numbers. Tests on an 858-style probe in a wind tunnel (Kaushagen, 1949) confirm that there is negligible crosstalk for the range $-10°$ to $+10°$.

c. *Computation of attack angle*

With the empirical values of k determined as a function of Mach number, we invert (7) and present calculated attack angles for the maneuver time period in Fig. 8. The agreement between the attack angles obtained from the Rosemount 858 probe and the radome is good: mean angles (over the 15-min period) differ by 0.2°, and the standard deviations are equal. From the time trace, there are no discernible differences in the signatures of the attack angles. This is also true for the period from 58 to 60 min that in Fig. 5 showed a discrepancy between ADIF and ADIFR. The computed angles of attack are identical because of the different Mach number dependencies of k for the two systems. During the period 58 to 60 min, M was increasing from 0.5 to 0.7. The attack angle variations during the two pitching maneuvers at $M = 0.4$ and 0.5 are due to induced aircraft vertical motion. The modulation of the vertical wind component during the pitching maneuvers, computed for both the radome and the 858 probe, is approximately the same.

d. *Frequency response*

The fast-response characteristics of the radome and 858 systems are presented in terms of spectra and phase-frequency plots to 12.5 Hz, the Nyquist frequency of the digital sampling system. The power spectra of the respective attack angle pressure differences for data in the turbulent boundary layer are shown in Fig. 9a (858) and 9b (radome). Since the sensitivity coefficients are different for each pressure measurement (see Fig. 5) the amplitudes of the spectra are also different. (The spectra of attack angle correspond approximately to those of vertical wind velocity at frequencies greater than ~1 Hz. At lower frequencies, airplane motions affect the attack angle). The 858 spectrum rolls off somewhat steeper than the

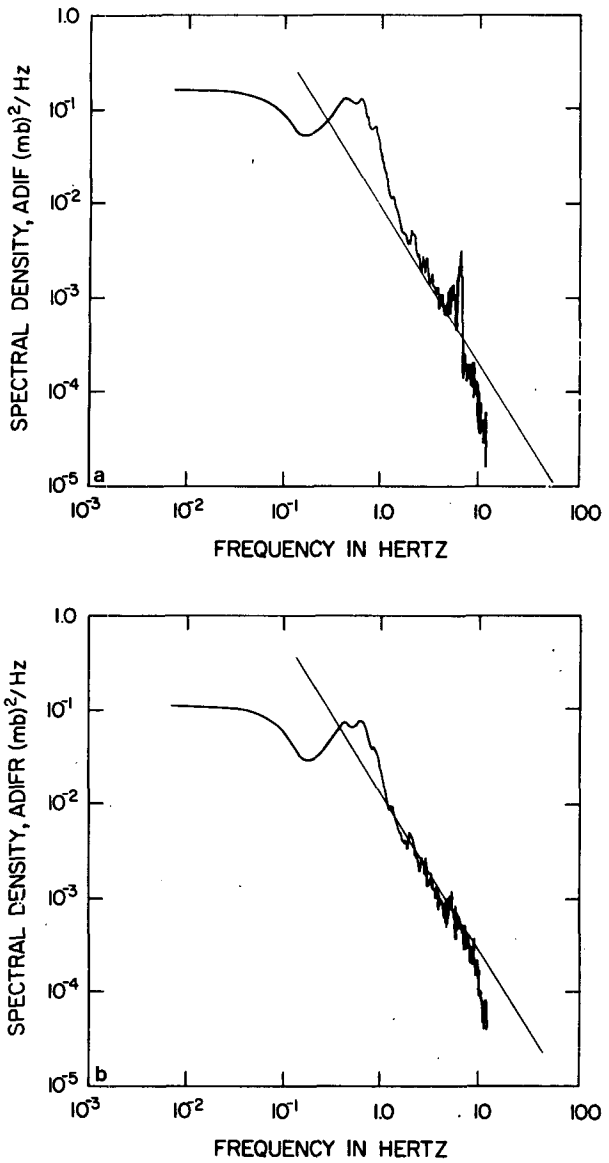

FIG. 9. Power spectrum of attack pressure difference fluctuations for (a) (ADIF), Rosemount 858 probe; (b) (ADIFR), Radome. Solid line is of slope $-5/3$.

$-5/3$ slope for the wind components predicted by turbulence theory (the Kolmogoroff inertial subrange) up to ~7 Hz. At 7 Hz, there is a sharp peak, due to the known vibration resonance of the Sabreliner nose boom. Beyond the peak, the spectrum falls sharply, due to damping of the pressure signal in the long (~4 m) lines between the 858 and its differential transducer. For the radome signal, the spectrum follows the $-5/3$ slope out to the cut-off of the low-pass data system filters (~10 Hz). There is a slight bump near 7 Hz that may be induced motion of the Sabreliner fuselage by the boom vibration. The phase shift, as a function of frequency, is shown in Fig. 10. We note that the radome system, with the short pressure lines, leads the 858 even at frequencies as low as 0.5 Hz, despite the fact that the radome is ~3.1 m downstream from the 858 probe. The dashed line is the expected shift due to the 3.1-m separation between the 858 and the radome. This does not take into account the difference in the pressure line lengths of the two systems.

To determine the effect of such long tube lengths on the response, flight tests were conducted with an NCAR Queen Air aircraft flying both the 858 and, for reference, a fixed-vane probe (Lenschow *et al.*, 1978) that has a much faster response time (on the order of 0.01 s) for both Pitot pressure and attack angle. The sensors were mounted at the same distance from the aircraft nose and displaced laterally by less than 20 cm. The tube lengths connecting the 858 pressure output lines with the transducers at the base of the boom were identical to those used on the Sabreliner. These tubes have an inside diameter (ID) of 0.432 cm. The ID of the flow angle ports is 0.16 cm; the Pitot port ID on the centerline of the probe is 0.40 cm. Pressure lines from these ports are routed internally through the probe with tubing of 0.36 cm internal diameter. The tests were conducted at a flight level of 790 mb, similar to the flight data of Fig. 10.

Spectra of the attack angle pressure difference showed little obvious indication of attenuation at high frequencies, or of a large resonance peak. (The Queen Air nose boom is considerably stiffer than the Sabreliner nose boom and consequently has a much higher resonant frequency with lower amplitude displacements.) Figs. 11 and 12 show that the phase angle of the 858 pitot pressure is approximately $\theta = -6f$ (de-

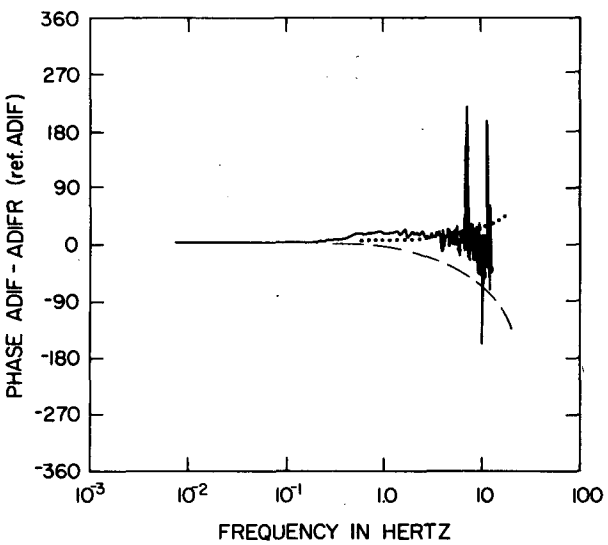

FIG. 10. Phase shift between attack pressure difference from Rosemount 858 probe (ADIF) and radome (ADIFR). Positive phase shift indicates radome leads the Rosemount 858. Dashed line: predicted phase shift due to longitudinal 3.1 m displacement between 858 and radome. Dotted line: predicted phase shift including effect of both longitudinal displacement and phase lag in 858 pressure lines.

grees), where f is frequency (Hz), and that the phase angle of the 858 attack angle pressure difference is $\theta = -9f$ (degrees), respectively.

We can compare these results with the theoretical results obtained by Iberall (1950) for the attenuation and phase lag of a pressure measurement at one end of a tube with an oscillating pressure applied at the other end. The theory takes into account compressibility and the volume of air contained in the instrument sensing chamber. However, it does not apply exactly to the 858 since the tubes are terminated at ports which have a smaller diameter than the tubes. We can make one simplification; the instrument volume is negligible compared with the tube volume.

Considering first the Pitot pressure tube, the theoretical results for a ratio of instrument volume to tube volume, $V_i/V_t = 0$, predict a phase lag of 22° at 10 Hz for an assumed tube diameter of 0.36 cm. At higher frequencies, the signal is attenuated and the phase shift continues to increase. The observed phase lag is ~60°. This considerable difference may be because the outside section of the tube is smaller in diameter than the main section. If we assume that this effectively changes V_i/V_t, we find that for a ratio of $V_i/V_t = 0.5$, $\theta = 60°$ at 10 Hz. Alternatively, we can calculate the effective diameter of a tube which has a 60° phase lag at 10 Hz. This turns out to be $d = 0.25$ cm.

For the attack angle differential pressure, if we use a tube diameter of 0.14 cm, the theoretical phase angle is ~90° at 10 Hz, which agrees well with the observed phase lag.

Obviously, the effect of a varying diameter in the pressure lines is significant. Since the theoretical results of Iberall (1950) do not cover such complex geometry, we can only use them for qualitative comparisons with the observed results. However, we can quantitatively apply the theoretical results to estimate what happens when we vary the geometry or the fluid properties. In particular, the Sabreliner typically flies at much higher altitudes than the altitude of these test results. The time constant of the pressure lines

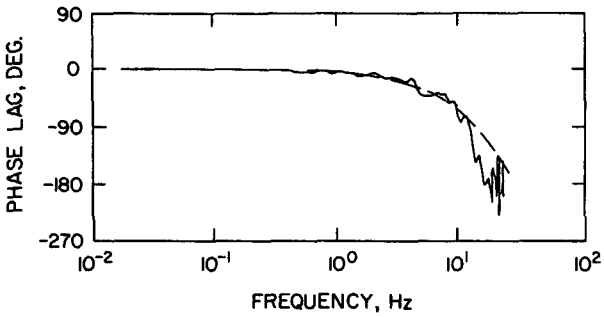

FIG. 11. Phase lag between fast-response Pitot and Rosemount 858 Pitot with 4.0-m tubing length. Results from Queen Air test flight. (Phase lag is defined here and in Fig. 12 so that negative angles mean that 858 is lagging reference.) Dashed line is the phase lag = $-6f$°, where f = frequency in Hz.

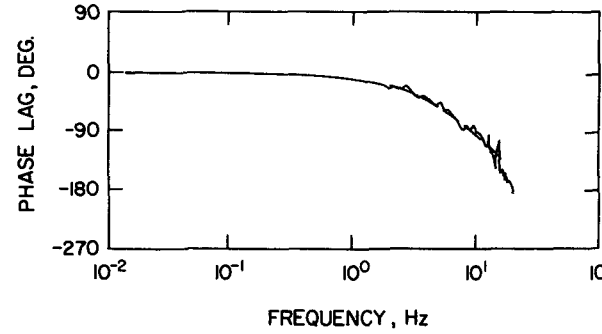

FIG. 12. Phase lag between attack angle fast-response vane and attack angle pressure difference Rosemount 858 probe (ADIF) with 4.0 m tubing length. Results from Queen Air test flight. Dashed line is the phase lag = $-9f$°, where f = frequency in Hz.

is inversely proportional to the static pressure. At 12.2 km in altitude, the atmospheric pressure is 188 mb. We add to this 80 mb for the Sabreliner pitot pressure. The ratio of the flight test pressure to this pressure is 3.06. Thus, at this level, the phase lags for Sabreliner measurements of true airspeed and incident flow angles are $-18f$° and $-27f$°, respectively. This can be a serious limitation when using the Sabreliner 858 probe air-motion data, particularly for calculating cospectra or covariances of turbulence data.

Applying the Queen Air test results to the radome test, the dotted line in Fig. 10 is the expected phase angle between the 858 and radome system, including both the time lag due to the downstream location of the radome and the observed phase lag in the 858 system due to the 3.1 m pressure line length. The measured phase angle agrees reasonably well with the prediction. This indicates that the radome system frequency response is superior to the 858 system as configured on the Sabreliner.

6. Discussion and conclusions

The tests presented in this paper have indicated that the use of pressure holes in the radome of a research aircraft is a promising air-motion measurement technique. Because of its simplicity, rigidity and noninterference with aircraft radar, it appears to have many advantages over sensors mounted on nose booms.

These tests have only been done over the Mach range 0.2–0.7, and only on a Sabreliner. Further tests are needed on different aircraft, especially at lower Mach numbers and on less streamlined propeller aircraft to determine how universal the technique is. We expect that it will work on other aircraft, as all that is basically required is a monotonic dependence of the pressure distribution with angle on the tip of the radome. The Reynolds number for even a very slow aircraft is still very large, so that the boundary layer approximation would apply well. There could pos-

sibly be pressure noise radiated from propellers that may degrade the system. Further tests are required on symmetrical radomes, particularly for determination of the sensitivity factor for sideslip angle.

The effects, if any, of upwash or flow streamline asymmetry at the radome nose have been accounted for in the *in-situ* calibration in the present study. Direct determination of upwash would involve detailed wind tunnel model studies. Therefore, in applying the present technique it is assumed that the upwash effect is a unique function of Mach number and is contained in the factor k.

Future design considerations on the radome system will focus on all-weather operation. Ice build-up will, of course, block the pressure holes on an unheated radome (this did occur on one flight with the present system). Options are to heat the radome electrically or with bleed air, as is done on a few research aircraft. The whole tip of the radome, even aft of the pressure holes, will have to be heated since ice build-up will change the shape and hence k, even if the holes are not blocked. Secondly, water ingestion into the pressure lines is another problem. For low-frequency applications, it may be possible to put in sufficient traps without seriously affecting response since the pressure lines are very short. Other schemes may be possible, such as back flushing the lines during flight with dry gas switched through a pressure multiplexing valve, heated diaphragms across the pressure holes, or flush-mounted transducers.

The frequency response characteristics of the present system are close to the limit of the pressure transducers used. Therefore, we could not determine the upper limit of frequency response (lower limit of eddy size) at which flow distortion effects may become significant.

A further result indicated by the present study is the refinement of the calibration of the 858-type probe. It was found that the *in-situ* values of k vs Mach numbers were lower than the theoretical or wind tunnel values. This result agrees with the few previous tests on this problem. It is suggested that *in-situ* calibrations be performed on other boom installations. Also, modern numerical flow-pattern calculation techniques would aid in placement of nose booms and analysis of such data.

Acknowledgments. We thank Lawrence Abbott and Robert Carl who assisted with the installation of the system on the Sabreliner. Robert Burris and Thomas McQuade were the flight crew for the tests. Special thanks are due Kenneth Hansen of the NCAR Scientific Computing Division, who performed the software analysis of the data.

The comments of John Wyngaard, Julian Hunt, James Telford, Jack Warner, Gavin Fisher and Manfred Reinhart during this investigation have been most helpful. The manuscript was typed by Peggy Taylor.

REFERENCES

Armistead, K. H., and L. D. Webb, 1973: Flight calibration tests of a nose-boom-mounted fixed hemispherical flow-direction sensor. NASA Tech. Note D-7461, 27 pp.

Britter, R. E., J. C. R. Hunt and J. C. Mumford, 1979: The distortion of turbulence by a circular cylinder. *J. Fluid Mech.*, **92,** 269–301.

Duncan, T. M., and R. C. Brown, 1978: A data acquisition system for airborne meteorological research. *Bull., Amer. Meteor. Soc.*, **59,** 1128–1134.

Durbin, P. A., and J. C. R. Hunt, 1980: On surface pressure fluctuations beneath turbulent flow round bluff bodies. *J. Fluid Mech.*, **100,** 161–184.

Eckert, B., 1938: Experiences with flow direction instruments. NASA Tech. Memo. 969, 10 pp.

Fischel, J., and L. D. Webb, 1964: Flight-informational sensors, display, and space control of the X-15 airplane for atmospheric and near-space flight missions. NASA Tech. Note D-2407, 27 pp.

Hunt, J. C. R., 1973: A theory of turbulent flow round two-dimensional bluff bodies. *J. Fluid Mech.*, **61,** 625–706.

Iberall, A. S., 1950: Attenuation of oscillatory pressures in instrument lines. *J. Res. Natl. Bur. Stand.*, **4J,** 85–108.

Kaushagen, W. M., 1949: Flight line computer. Rep. IH-431-P-28, Cornell Aeronautical Laboratory, Buffalo, NY, 244 pp.

Larson, T. J., and P. M. Siemers, 1978: Subsonic investigation of an all flush orifice air data system. NASA Tech. Note 4351, 95 pp.

Lawson, R. P., 1979: A system for airborne measurement of vertical air velocity. *J. Appl. Meteor.*, **18,** 1363–1368.

Lenschow, D. H., 1972: The measurement of air velocity and temperature using the NCAR Buffalo aircraft measuring system. NCAR Tech. Note/EDD-74, 39 pp.

——, 1976: Estimating updraft velocity from an airplane response. *Mon. Wea. Rev.*, **104,** 618–627.

——, C. A. Cullian, R. B. Friesen and E. N. Brown, 1978. The status of air motion measurements on NCAR aircraft. *Preprints Fourth Symp. on Meteorological Observations and Instrumentation*, Denver, Amer. Meteor. Soc., 433–438.

McFadden, N. M., G. A. Rathert and R. S. Bray, 1952: Flight calibration of angle of attack and sideslip detectors on the fuselage of a 35° swept wing fighter aircraft. NASA RMA52A04, 26 pp.

Montoya, E. J., 1973: Wind-tunnel calibration and requirements for in-flight use of fixed hemispherical head angle-of-attack and angle-of-sideslip sensors. NASA Tech. Note D-6986, 45 pp.

Rogal, B., 1964: *In-flight Test Instrumentation,* M. A. Perry, Ed., Pergamon Press, 22 pp.

Vornwald, W. H., 1968: An introduction to the Rosemount Engineering Co. Model 858 flow angle sensor. REC Rep. 56822A, Rev. A., Minneapolis, 9 pp.

Wyngaard, J. C., 1981: The effect of probe-induced flow distortion on atmospheric turbulence measurements. *J. Appl. Meteor.*, **20,** 784–794.